Testing shell-model interactions at high excitation energy and low spin: Nuclear resonance fluorescence in ^{74}Ge

S. R. Johnson,[1,2,*] R. V. F. Janssens,[1,2] U. Friman-Gayer,[1,2,†] B. A. Brown,[3,4] B. P. Crider,[5] S. W. Finch,[6,2] Krishichayan,[6,2] D. R. Little,[1,2] S. Mukhopadhyay,[7,‡] E. E. Peters,[7] A. P. D. Ramirez,[7,§] J. A. Silano,[8] A. P. Tonchev,[6,8] W. Tornow,[6,2] and S. W. Yates[7]

[1]*Department of Physics and Astronomy, University of North Carolina at Chapel Hill, Chapel Hill, North Carolina 27599, USA*
[2]*Triangle Universities Nuclear Laboratory, Duke University, Durham, North Carolina 27708, USA*
[3]*Facility for Rare Isotope Beams, Michigan State University, East Lansing, Michigan 48824, USA*
[4]*Department of Physics and Astronomy, Michigan State University, East Lansing, Michigan 48824, USA*
[5]*Department of Physics and Astronomy, Mississippi State University, Mississippi State, Mississippi 39762, USA*
[6]*Department of Physics, Duke University, Durham, North Carolina 27708, USA*
[7]*Department of Chemistry and Physics and Astronomy, University of Kentucky, Lexington, Kentucky 40506, USA*
[8]*Nuclear and Chemical Sciences Division, Lawrence Livermore National Laboratory, Livermore, California 94550, USA*

(Received 17 July 2023; accepted 28 July 2023; published 21 August 2023)

With their complex low-spin structure, the germanium isotopes have accrued a large number of experimental data which challenge nuclear models. The structure of the ^{74}Ge isotope is investigated here with nuclear resonance fluorescence as part of an extensive campaign of experimental tests of the shell model in the germanium isotopic chain using a number of complementary techniques. Levels were excited with 3.10–5.44 MeV photon beams provided by the High Intensity Gamma-Ray Source at TUNL. Many new levels were identified and their spins, parities, branching ratios, and associated scattering cross section values were determined. Large-scale shell-model calculations, which include jj44b and JUN45 effective interactions developed to describe nuclei in this mass region, predict the new data satisfactorily. This study extends the validation of these two interactions, which are candidates for computation of matrix elements to be used in the interpretation of neutrinoless double-β decay experiments in ^{76}Ge, into the low-spin, high excitation energy domain.

DOI: 10.1103/PhysRevC.108.024315

I. INTRODUCTION

The low-spin structure of the even-even germanium isotopes has been the focus of many experimental studies in recent years, including γ-ray spectroscopy, multinucleon transfer reactions, and β decay, as well as many theoretical investigations, described in detail in Refs. [1,2] and references therein. Moreover, rich level structures in the germanium isotopes and interest in the neutrinoless double-beta decay process ($0\nu\beta\beta$) in ^{76}Ge have sparked renewed explorations of this isotopic chain.

The systematics of the low-spin excited states in the even-even germanium isotopes highlights complex shape phenomena for an isotopic chain with only four valence protons above the $Z = 28$ shell gap. The stable even-even germanium isotopes all have a low-lying 0_2^+ state with an associated structure different from that of the 0_1^+ ground state. The energy of this 0_2^+ state decreases with increasing neutron number from $N = 36$ to $N = 40$, reaching a minimum and becoming the first excited state in ^{72}Ge, a rare occurrence anywhere in the nuclear chart. The 0_2^+ level increases in energy again between $N = 42$ and $N = 44$. Closer inspection with multinucleon transfer reactions and Coulomb excitation revealed a transition in the ground-state shape from oblate to prolate between $N = 38$ and $N = 40$, which is interpreted as an exchange in character between the 0_1^+ and excited 0_2^+ levels [3,4]. Calculations using several theoretical perspectives, such as those done in the Hartree-Fock-Bogoliubov framework by Nomura, Rodríguez-Guzmán, and Robledo [5] and those in the covariant density functional theory by Ait Ben Mennana *et al.* [6], display multiple minima in potential energy surfaces as a function of deformation parameters, lending further credence to the possibility of coexisting shapes. Moreover, ^{72,74}Ge are isotones of ^{68,70}Ni, in which the phenomenon of shape coexistence and similarly low-lying excited 0^+ states have recently come into focus [7].

A maximum in the energy of the 2_1^+ state is anticipated at the $N = 40$ subshell closure in ^{72}Ge. Instead, it is seen at $N = 38$ in ^{70}Ge, which may indicate a breaking of the $N = 40$ subshell closure related to the presence of an island of inversion in nuclei of this region around the "doubly-magic" nuclei ^{68}Ni and ^{78}Ni [8,9].

*sjohnson@unc.edu
†Present address: European Spallation Source ERIC, Lund, Sweden.
‡Present address: Nuclear and Radiological Engineering and Medical Physics Program, Georgia Institute of Technology, Atlanta, Georgia 30332, USA.
§Present address: Nuclear and Chemical Sciences Division, Lawrence Livermore National Laboratory, Livermore, California 94550, USA.

These even-even Ge isotopes also have in common a low-lying 2_2^+ γ-band head, which decreases in energy with increasing N, suggestive of triaxiality. Recent Coulomb excitation experiments provide supporting evidence for this interpretation in the even-even neighbors of ^{74}Ge [10–14]. Numerous variations of the shell model [15–17], Monte Carlo shell model [18], projected shell model [19], and triaxial projected shell model [20] have been deployed to describe the germanium isotopes. Collectivity has been introduced with the Hartree-Fock-Bogoliubov approach [5,21], the interacting boson model [22], and covariant density functional theory [6,23]. These approaches have each been able to successfully predict some observables, but overall there remains little consensus about the results of the various calculations. Hence, the germanium isotopes continue to be a testing ground for nuclear theory and a challenge to interpret.

As well as being important in the context of the structural evolution in the isotopic chain, the structure of ^{74}Ge has implications for the $0\nu\beta\beta$ process in ^{76}Ge. The $0\nu\beta\beta$ matrix elements in ^{76}Ge can be represented as a sum over states in ^{74}Ge, including a two-nucleon transfer component [24,25]. Understanding which interaction best describes the excited states in ^{74}Ge should improve these calculations.

Here, we report on a study of ^{74}Ge over an extended range in excitation energy using nuclear resonance fluorescence (NRF) with the aim of both understanding the photoresponse of low-spin excited states and of testing the ability of different shell-model interactions to describe the states and their de-excitation modes. It should be noted that the present collaboration has also recently studied excited states in ^{74}Ge with angular momentum up to $J = 6\hbar$ and up to an excitation energy of ∼3 MeV using inelastic neutron scattering at the University of Kentucky Accelerator Laboratory [26]. With NRF as a complementary probe, knowledge of low-spin states is extended to ∼5.5 MeV excitation with a focus on *E1* and *M1* strengths. With this approach, the low-spin states and their decay paths are cataloged in the energy range spanned by the experiment, quantifying the associated multipolarity and scattering cross sections, and comparing the data with results of shell-model calculations. An NRF measurement for ^{76}Ge was also recently published [27].

Levels in this energy range in ^{74}Ge have been studied previously using NRF [28,29]. These investigations found several spin-1 states in the region of interest. However, the previous measurements were not able to discern information about the associated decay paths or multipolarities in most cases, and there remain regions where no low-spin states are known.

II. METHODS

The NRF technique, described extensively in Ref. [30], was used to study the photoresponse of ^{74}Ge in a range of energies. This experiment was conducted at the High Intensity γ-Ray Source (HIγS) facility located at the Triangle Universities Nuclear Laboratory (TUNL). HIγS provided quasi-monoenergetic, linearly polarized γ-ray beams at 16 energy settings between 3.10 and 5.44 MeV with a relative full width at half-maximum (FWHM) of about 3% [31]. The ^{74}Ge target consisted of germanium dioxide powder, isotopically

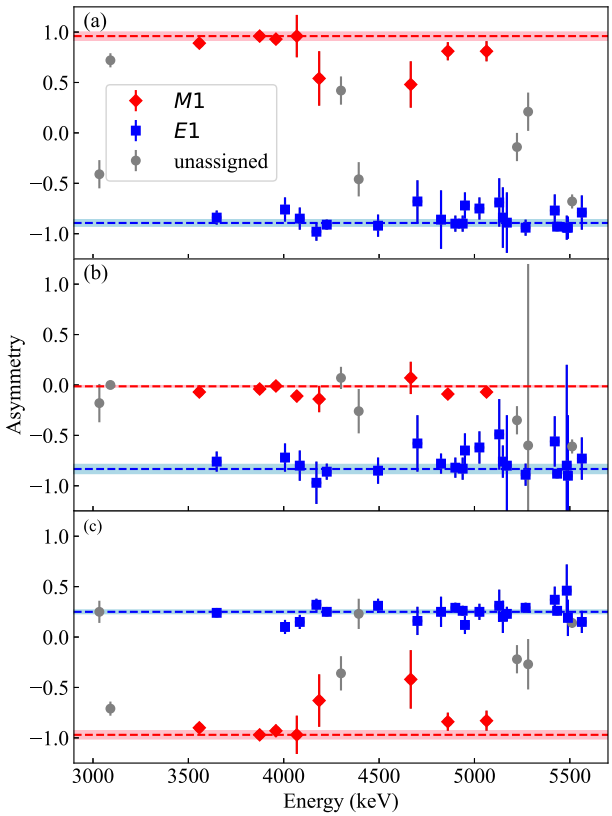

FIG. 1. Experimental asymmetries (a) $\Sigma_{\parallel,\perp,\mathrm{exp}}$, (b) $\Sigma_{\parallel,\mathrm{back,exp}}$, and (c) $\Sigma_{\perp,\mathrm{back,exp}}$ compared to calculated theoretical values with estimated adjustment for solid-angle effects. Red diamonds represent transitions determined to be of $M1$ character and blue squares $E1$ character. Unassigned multipolarities are represented by grey circles. See text for details.

enriched to 98.90(5)%, weighing 8.968(5) g with a thickness of 1.91 cm. The target nuclei were excited by the HIγS beam and the fluorescent radiation emitted was measured. Data were accumulated for 4–6 h at each lower energy setting and 6–7 h for each higher energy one.

Using a nearly 100% linearly polarized beam allows the multipolarity of the emitted radiation to be distinguished by measuring the relative intensity of the photons at several angles around the target. The angular momenta and parities of excited states can then be inferred from the measured angular correlations [30]. The relatively small energy spread of the quasi-monoenergetic HIγS beam also enables measurements of branching ratios without ambiguity, as opposed to experiments using bremsstrahlung radiation, which populate excited states across a broad energy range.

Data were taken using the γ^3 setup at HIγS [32], consisting of six high-purity germanium (HPGe) detectors placed at angles suitable to distinguish between photons of different multipole character, taking advantage of the >99% linear polarization of the beam [31,33]. A schematic showing key detector positions can be found in Fig. 1 of Ref. [33], which also provides additional information on the setup. Detectors

TABLE I. Calculated asymmetries of interest for elastic transitions calculated using the formalism described by Iliadis and Friman-Gayer [38].

Transition	$\Sigma_{\parallel,\perp}$	$\Sigma_{\parallel,\text{back}}$	$\Sigma_{\perp,\text{back}}$
$0^+ \to 1^- \to 0$	−1	−1	0.333
$0^+ \to 1^+ \to 0$	1	0	−1
$0^+ \to 2^+ \to 0$	1	1	0

in the plane perpendicular to the propagation of the beam (polar angle $\theta = 90°$) measuring the radiation field parallel (azimuthal angle $\phi = 0°, 180°$) and perpendicular ($\phi = 90°, 270°$) to the beam polarization can be used to distinguish between transitions of electric and magnetic character. Detectors at a backward angle ($\theta = 135°$, $\phi = 0°, 180°$) can distinguish sequences of the type $0^+ \to 1^+ \to 0$ from those of the type $0^+ \to 2^+ \to 0$. Distinguishing between transitions of the type $0^+ \to 1^- \to 0$ and $0^+ \to 2^- \to 0$ would require a perpendicular backward-angle detector (e.g., $\theta = 135°$, $\phi = 90°$), which was not available during this measurement.

HPGe detectors were calibrated using standard ^{56}Co and ^{152}Eu radioactive sources. Additionally, a sample of ^{137}Cs was placed near the detectors for the duration of the experiment, giving a continuous energy calibration point at 662 keV, as well as an indirect measure of the data acquisition dead time. For energy calibrations beyond 3.5 MeV (the highest-energy γ ray from ^{56}Co decay), γ rays from transitions of previously measured excited states in ^{12}C (the level at 4440 keV) [34], a common contaminant, and ^{74}Ge (levels listed in Table II) [35] were used. Relative efficiency calibrations were performed using the previously mentioned calibration standards with the RADWARE software package [36].

The energy profile of the photon beam was measured with a HPGe detector that was moved into the beam line, downstream of the target, after suitable attenuation of the incoming photon flux.

Energies E_i for the states excited in NRF were Doppler- and recoil-corrected as described by

$$E_i = E_\gamma\left(1 + \frac{E_\gamma}{2Mc^2}(1 - 2\cos\theta)\right), \tag{1}$$

where E_γ is the energy of the ground-state transition measured by the detectors at polar angle θ and M is the mass of the nucleus [37]. This correction is on the order of 0.5 to 1 keV under the present experimental conditions. For each excited state, the reported level energies represent an error-weighted average of the energies measured by each of the six detectors with a statistically significant (3σ) yield. Therefore, the uncertainty in each reported E_i value is dependent on the uncertainty of the energy calibration of the detectors in which the transition was observed.

Experimental asymmetries are reported for each transition. This quantity is defined as

$$\Sigma_{a,b} = \frac{A(\theta_a, \phi_a) - A(\theta_b, \phi_b)}{A(\theta_a, \phi_a) + A(\theta_b, \phi_b)}, \tag{2}$$

where $A(\theta_{a,b}, \phi_{a,b})$ are the yields in detectors at positions a and b, respectively. The experimental asymmetry is related to the angular correlation function of the transition in question. This relationship is described in detail in Refs. [30,38].

Experimental asymmetry values are reported in this work for pairs of detectors at three different positions, i.e., for every combination of the parallel ($\parallel$), perpendicular ($\perp$), and at backward-angle $\theta = 135°$ ("back") positions. Detectors in symmetric positions with respect to the beam direction are generally combined due to the symmetry of the angular distributions. In cases where the same elastic transition is observed using adjacent photon beam energy settings, the spectra of both measurements are summed to determine values for E_γ, E_i, and each Σ.

To determine the multipolarity of a transition, the experimental asymmetries are compared to a values calculated using the angular correlation formalism described in Ref. [38]. In this framework, the expected asymmetry for a transition with associated angular correlation function $W(\theta, \phi)$ can be expressed as

$$\Sigma_{a,b} = \frac{W(\theta_a, \phi_a) - W(\theta_b, \phi_b)}{W(\theta_a, \phi_a) + W(\theta_b, \phi_b)}. \tag{3}$$

Angular momentum and parity J^π, are assigned following a χ^2_{red} analysis of the experimental asymmetries in comparison to the theoretical values for the most-likely transition sequences shown in Table I, but with a corrections for detector solid-angle effects estimated by measuring the asymmetry for the ground-state decay of excited states in ^{74}Ge with prior independent firm J^π assignments, namely the 1^- states at 3647, 4225, and 5435 keV, and the 1^+ state at 3875 keV. A J^π assignment was proposed for each state based on the comparison with the corrected theoretical asymmetry yielding the smallest χ^2_{red} value. As illustrated in Fig. 1, firm assignments were not made for states with ambiguous asymmetries or suspected contaminant peaks. Figure 2 provides spectra of the ground-state decay of two excited levels measured in parallel and perpendicular detectors, illustrating the cleanliness with which J^π assignments can be made when using NRF with linearly polarized photon beams. For inelastic transitions, i.e., transitions feeding excited states in ^{74}Ge from the level populated by photoabsorption, the energy is reported for $\theta = 90°$ and 135° detectors separately, but with an error-weighted average for detectors in symmetric positions, because the recoil correction is θ-dependent. These transitions are placed based on their measured energy being within 1–2 keV of the difference between the excitation energies of the feeding and final states.

Multipole mixing ratios of inelastic transitions are calculated by comparing the experimental asymmetries to those predicted theoretically for the excitation and decay path $0^+ \to J^\pi_i \to J^\pi_f$, where the mixing ratio δ is a continuous variable ranging from −100 to 100, approximating the possible physical range from $-\infty$ to ∞, and a χ^2 analysis is performed. Theoretical asymmetries for selected values of δ are displayed in Fig. 3, again calculated using the formalism described in Ref. [38]. This calculation is only attempted for a given inelastic transition when J^π_i and J^π_f are known. The range of experimental mixing ratios reported here are those bounded

TABLE II. Experimental asymmetry of electromagnetic radiation corresponding to elastic transitions measured in ^{74}Ge as seen by parallel, perpendicular, and backward-angle detectors (see text for details).

Beam energy (MeV)	E_{level} (keV)	I_s (eVb)	$\Sigma_{\parallel,\perp}$	$\Sigma_{\parallel,\text{back}}$	$\Sigma_{\perp,\text{back}}$	J^π	Notes
3.10	3033.5(4)	11.7(5)	−0.41(14)	−0.18(19)	0.25(11)	$1^{(-)}$	a
	3091.22(30)	10.5(15)	0.72(7)	0.00(4)	−0.71(7)	$1^{(+)}$	b,c
3.60	3558.0(4)	16.9(14)	0.89(5)	−0.07(2)	−0.90(5)	1^+	b
	3648.48(22)	9.8(11)	−0.84(7)	−0.76(10)	0.24(4)	1^-	b
3.90	3874.9(3)	43.4(26)	0.96(4)	−0.04(2)	−0.97(4)	1^+	b,d,e
	3960.12(13)	18.6(15)	0.93(5)	−0.01(3)	−0.93(6)	1^+	b,e
4.03	3874.9(3)	43.4(26)	0.96(4)	−0.04(2)	−0.97(4)	1^+	b,d,e
	3960.12(13)	18.6(15)	0.93(5)	−0.01(3)	−0.93(6)	1^+	b,e
	4006.3(4)	4.5(9)	−0.76(12)	−0.72(14)	0.10(7)	1^-	b
	4069.7(5)	5.1(10)	0.96(21)	−0.11(6)	−0.97(19)	1^+	b
	4084.49(31)	6.5(10)	−0.85(11)	−0.80(15)	0.15(7)	1^-	b
4.18	4171.16(28)	11.0(13)	−0.98(9)	−0.97(21)	0.32(6)	1^-	b
	4186.4(6)	1.88(27)	0.54(27)	−0.14(13)	−0.63(26)	1^+	
	4225.58(21)	28.4(24)	−0.91(5)	−0.86(8)	0.25(3)	1^-	b,e
4.34	4225.58(21)	28.4(24)	−0.91(5)	−0.86(8)	0.25(3)	1^-	b,e
	4301.1(6)	12.8(20)	0.42(14)	0.07(11)	−0.36(17)	$1^{(+)}$	b
	4392.1(6)	2.5(7)	−0.46(17)	−0.26(22)	0.23(15)	$1^{(-)}$	
4.51	4493.9(5)	6.9(9)	−0.92(11)	−0.85(13)	0.31(7)	1^-	b
4.68	4669.5(7)	0.71(24)	0.48(23)	0.07(16)	−0.42(29)	1^+	
	4700.7(6)	1.3(8)	−0.68(21)	−0.58(28)	0.16(14)	1^-	
4.86	4825.75(31)	10.7(7)	−0.86(29)	−0.78(10)	0.25(15)	1^-	
	4862.3(6)	7.0(12)	0.81(9)	−0.09(5)	−0.84(9)	1^+	b
	4900.42(30)	13.0(22)	−0.90(8)	−0.82(10)	0.29(5)	1^-	b
	4938.66(30)	17.9(18)	−0.90(8)	−0.83(11)	0.26(5)	1^-	b
	4949.9(5)	8.1(12)	−0.72(13)	−0.65(17)	0.12(9)	1^-	b
5.05	5025.1(5)	9.1(21)	−0.75(11)	−0.62(16)	0.25(8)	1^-	
	5064.4(6)	10(4)	0.81(10)	−0.07(5)	−0.83(10)	1^+	
	5129.0(7)	6.2(16)	−0.69(24)	−0.49(35)	0.31(16)	1^-	b
	5148.1(4)		−0.84(30)	−0.76(16)	0.20(16)	1^-	e
	5170.7(4)		−0.89(30)	−0.83(46)	0.23(7)	1^-	e
5.24	5148.1(4)	7.5(7)	−0.84(30)	−0.76(16)	0.20(16)	1^-	e
	5170.7(4)	7.4(7)	−0.89(30)	−0.83(46)	0.23(7)	1^-	e
	5224.5(5)	1.62(28)	−0.14(14)	−0.35(14)	−0.22(14)	$1^{(-)}$	
	5268.84(29)	24.6(22)	−0.94(8)	−0.89(11)	0.29(5)	1^-	b
	5283.2(9)		0.21(19)	−0.6(18)	−0.27(25)	$1^{(+)}$	f
5.44	5420.5(8)	7.8(14)	−0.77(16)	−0.56(25)	0.37(13)	1^-	b
	5434.8(5)	91(6)	−0.93(4)	−0.88(4)	0.26(2)	1^-	b,d
	5484.2(7)	20.4(28)	−0.94(12)	−0.8(10)	0.46(26)	1^-	b
	5490.6(7)	27(3)	−0.94(11)	−0.9(6)	0.19(18)	1^-	b
	5514.8(8)	22.2(27)	−0.68(7)	−0.61(7)	0.14(5)	$1^{(-)}$	b,d
	5563.0(5)	12.0(16)	−0.79(17)	−0.73(21)	0.15(11)	1^-	

[a] I_s adopted from Ref. [28].
[b] I_s adopted from Ref. [29].
[c] A state at 3089 keV in ^{72}Ge with $\Gamma = 1.2(6)$ eV [40] may interfere with the 3091-keV state in ^{74}Ge with $\Gamma = 0.0104(11)$ eV [35], despite the low ^{72}Ge abundance in the target.
[d] Used in energy calibration procedures. E_i adopted from Ref. [35].
[e] E_{level} and Σ from combined data at two photon beam energies.
[f] Possible interference from ^{72}Ge.

by the $\chi^2_{\text{min}} + 1$ surface, with the limits of that surface corresponding to one standard deviation in δ.

The energy-integrated scattering cross section, described in Ref. [30], is given by

$$I_{s,f} = \frac{2J_0 + 1}{2J_i + 1}\left(\frac{\pi\hbar c}{E_i}\right)^2 \frac{\Gamma_0\Gamma_f}{\Gamma}, \tag{4}$$

where Γ is the total width, and Γ_0 and Γ_f are the partial decay widths to the ground and final state f.

For elastic transitions, the integrated scattering cross section reduces to

$$I_{s,0} = \frac{2J_0 + 1}{2J_i + 1}\left(\frac{\pi\hbar c}{E_i}\right)^2 \frac{\Gamma_0^2}{\Gamma}. \tag{5}$$

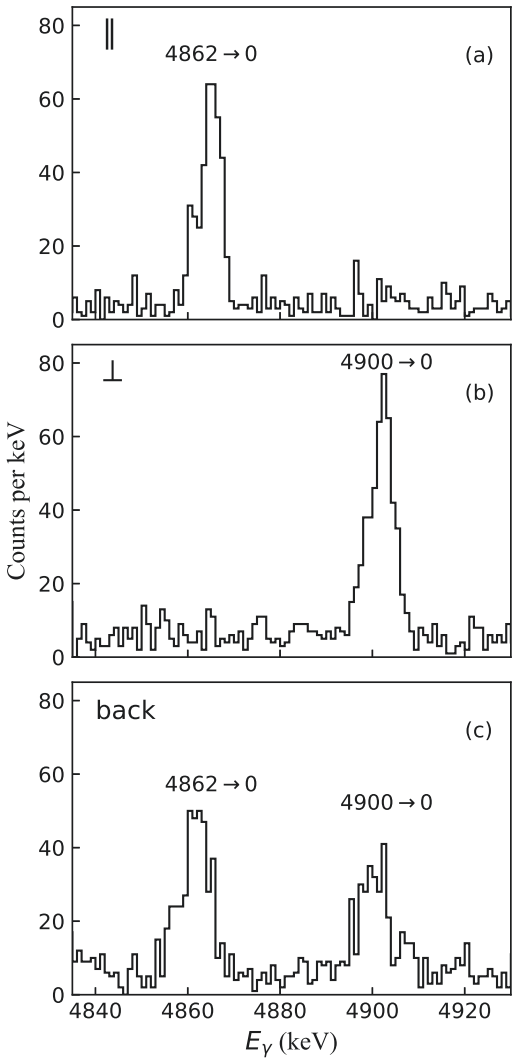

FIG. 2. Spectra measured at a beam energy of 4.86 MeV, showing ground-state transitions from excited states at 4862.3(6) and 4900.42(30) keV in ^{74}Ge as seen by detectors (a) parallel and (b) perpendicular to the beam polarization as well as (c) at a backward-angle. The difference between transitions of *M1* (a) and *E1* (b) character is clearly apparent.

Integrated scattering cross-section data are computed by comparing the relative beam intensity at the energy of each excited state with integrated cross section data from a bremsstrahlung experiment reported by Massarczyk *et al.* [29] in order to estimate the incident photon flux at the corresponding resonance energies. This procedure is possible only when states with reference data and new states of interest are both excited using the same photon beam setting and their decays are observed simultaneously. Relative beam intensities were obtained by reconstructing the incident photon spectra measured at each beam energy with the large-volume HPGe detector positioned directly into the beam. This procedure involved simulating the detector response using GEANT4 in the same manner as in Ref. [39].

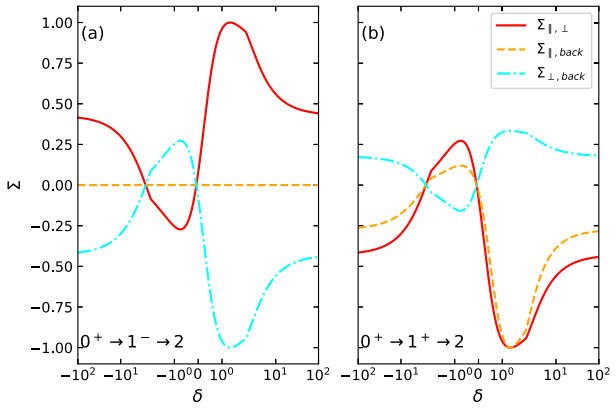

FIG. 3. Calculated asymmetries as a function of mixing ratio δ for transitions of the type (a) $0^+ \to 1^- \to 2$ and (b) $0^+ \to 1^+ \to 2$.

For a transition from state i to state f in a given detector, the yield is given by

$$A \propto W(\theta, \phi)\epsilon(E_\gamma)I_{s,f}\Phi_\gamma(E_i), \tag{6}$$

where $\Phi_\gamma(E_i)$ is the flux of the photon beam at energy E_i and $\epsilon(E_\gamma)$ is the efficiency of the detector at energy E_γ, as described in Ref. [39]. After integrating in time over the duration of a measurement, the total area in peaks α and β corresponding to two different elastic transitions excited at the same photon beam energy can be compared:

$$\frac{\Phi_\gamma(E_\alpha)}{\Phi_\gamma(E_\beta)} = \frac{A_\alpha W_\beta \epsilon(E_{\gamma,\beta})I_{s,0,\beta}}{A_\beta W_\alpha \epsilon(E_{\gamma,\alpha})I_{s,0,\alpha}}. \tag{7}$$

The value $\frac{\Phi_\gamma(E_\alpha)}{\Phi_\gamma(E_\beta)}$ is measured by taking the ratio of the relative beam intensities at the level energies E_α and E_β from the reconstructed beam spectrum. If $I_{s,0,\alpha}$ has been measured elsewhere, then $I_{s,0,\beta}$ can be determined. Integrated scattering cross-section results were determined in this manner, using data from Ref. [29] as $I_{s,0,\alpha}$ inputs. If several transitions with reference data were available, the reported $I_{s,0,\beta}$ is a weighted average of each resulting value.

In the case of the levels excited by the 4.68-MeV photon beam, no reference transitions were available from Ref. [29]. Instead, data from the next-highest beam energy at 4.86 MeV was used to obtain the relative beam flux. The flux was normalized using the area of the peak corresponding to beam photons which had been Compton-scattered by the target. By comparing the area of this peak in the 4.68- and 4.86-MeV measurements, along with information about the integrated scattering cross section of one excited state seen at 4.86 MeV, the relative flux was obtained and results for the integrated scattering cross section for the states measured at 4.68 MeV were determined. As the Compton scattering cross section is angle-dependent, the geometric effect of detector solid angles is estimated to contribute an additional 40% to the uncertainty in this determination.

III. RESULTS

The elastic transitions from the 36 $J = 1$ states observed in this experiment are listed in Table II, where they are grouped by the nominal energy of the beam at which they were excited. Note that only beam energies at which γ rays from ^{74}Ge were observed are listed in this table. For example, no transitions were seen at photon beams with nominal energies of 3.22, 3.34, 3.47, or 3.74 MeV and, consequently, nothing is reported in Table II. Experimental asymmetries and resulting J^π determinations are listed as well.

Energies of some known ground-state transitions in ^{74}Ge were used as input for energy calibrations. Therefore, updated level or γ-ray energies for these excited states are not reported. Rather, the values from Ref. [35] were adopted and these cases are also indicated in Table II.

Nine new I_s values are determined in this experiment. To provide a complete picture of the elastic scattering cross sections for the $J = 1$ states in the energy region spanned by the measurements, Table II also lists the I_s values from Ref. [29], which were used as input in the calculations, and one I_s value for the state at 3034 keV from Ref. [28], which was not measured in Ref. [29]. The present experiment was sensitive to spin-1 states with $I_{s,0}$ values as low as 0.71(24) eVb for the level at 4670 keV, where the lowest $I_{s,0}$ value measured in Ref. [29] was 2.8(10) and 2.8(9) eVb for the levels at 4853 and 4980 keV, and 0.4(1) eVb for the level at 2404 keV in Ref. [28].

The properties of the 20 inelastic transitions measured in this work are cataloged in Table III, including multipole mixing ratios for 16 of these. Most of these transitions could be identified as feeding the 2_1^+ or 2_2^+ excited states. Transitions through the pathway $0^+ \rightarrow 1^\pm \rightarrow 2^+$ have angular distributions which vary depending on δ, the multipole mixing ratio. Hence, the asymmetry exhibited by these γ rays was not used to deduce information about the emitting state. Rather, energy differences between the $J = 1$ states excited directly in the NRF process and known lower-lying excited levels were used to determine the placement of the inelastic transitions in the decay process. Armed with the knowledge of the spins and parities of all the levels, the asymmetries are then used to determine the associated δ values.

Although most inelastic transitions were identified as feeding the lowest-lying 2^+ levels, one γ ray with energy 3688 keV was identified as feeding the 0_2^+ level at 1483 keV from the 1^- state at 5170 keV. Its measured asymmetry matches very closely the asymmetry expected for the $0^+ \rightarrow 1^- \rightarrow 0$ sequence, i.e., with the anticipated angular distribution given in Table I.

All the results from the present measurements are combined to produce an overarching picture of the low-spin structure of ^{74}Ge in Table IV. This table includes information about the electromagnetic decay(s) of each state seen in this work, including branching ratios for the observed decay paths and J^π values. Newly observed excited states and decay branches are highlighted. Sixteen ambiguities in J^π values have been resolved and nine new J^π assignments are proposed for previously unobserved $J = 1$ states. The following 11 newly observed excited states are concentrated in the 4.186–5.283 MeV region: 4186, 4392, 4670, 4701, 4826, 5025, 5064, 5148, 5171, 5225, and 5283 keV.

While previous NRF experiments have reported several of the excited states observed here, significant additional information in the form of new decay paths has now been added. Almost all inelastic transitions, 18 out of the 20 studied in this work, had not been reported earlier. This is possible because of the quasi-monochromaticity of the photon beam, which allows excitation of the states of interest in isolation relative to the lower-lying levels toward which they decay. The parities of many excited states could also be determined in many instances where this was impossible in previous works by taking advantage of the linear polarization of the beam.

The parities of only the following five excited states in this energy range had been determined previously using NRF [35]: 3648, 3875, 4085, 4225, and 5435 keV, all of which were measured in Ref. [28]. The present parity determinations disagree with these previous works only for the excited state at 4084 keV, where the previous proposed 1^+ assignment is in contradiction with the present 1^- determination based on the experimental asymmetries agreeing well with those of an $E1$ transition. Ambiguities in parity are resolved for most other excited states observed earlier, 16 in total, the strongest of which is the 5491-keV state with $I_{s,0} = 27(3)$ eVb and the weakest of which is the 4006-keV level with $I_{s,0} = 4.5(9)$ eVb. Nevertheless, some instances remain where experimental asymmetries are ambiguous and no firm assignment can be proposed. In some of these cases, interference from a small amount of ^{72}Ge in the target sample is suspected. This applies to the 3091-keV level, where a strong $J = 1$ excited state is known nearby in ^{72}Ge, and is suspected to apply to the 5283-keV level as well.

IV. DISCUSSION

As can be inferred from Table IV, the NRF measurements presented here have established 11 new $J^\pi = 1^\pm$ states relative to the most recent work of Ref. [29], and added 22 levels relative to the latest ENSDF compilation [35]. For 29 of the 36 states studied, firm J^π assignments are now available.

The 3.1–3.6 MeV measurements were planned in part to cover the highest energies observed in an $(n, n'\gamma)$ experiment carried out at the University of Kentucky Accelerator Laboratory [26]. As discussed in Sec. I, these measurements are complementary and are part of an attempt to characterize excitation modes of ^{74}Ge as extensively as possible. The four $J = 1$ levels of Table IV at 3034, 3091, 3558, and 3649 keV are observed both in this work and in the work of Ref. [26] and, in all cases, asymmetries measured here are consistent with the spins and parities proposed in the latter work. However, while the J^π values for the last two states are firm and confirm the neutron scattering results, for the first two, the accuracy of the measured asymmetries is insufficient for firm assignments. Furthermore, Ref. [26] observed a $J = 1$ level at 3276 keV, which was not observed in this measurement.

As can be seen in Table IV, for the 3091- and 3558-keV states, de-excitation paths to the 2_2^+ and 2_1^+ levels, respectively, are confirmed as well, although a precise branching ratio for the former level is hampered by the presence of

TABLE III. Same as Table II, but for inelastic transitions.

Beam energy (MeV)	$E_\gamma(90^\circ)$ (keV)	$E_\gamma(135^\circ)$ (keV)	$\Sigma_{\parallel,\perp}$	$\Sigma_{\parallel,\text{back}}$	$\Sigma_{\perp,\text{back}}$	Origin	Transition type	δ
3.10	1888.60(34)	1888.0(5)	0.08(21)	0.03(13)	−0.06(22)	3091→1204	$0^+ \to 1^- \to 2_2^+$	$-2.2^{+1.0}_{-1.4}$
								$-0.13^{+0.16}_{-0.27}$
							$0^+ \to 1^+ \to 2_2^+$	$-3.5^{+1.7}_{-6.2}$
								$0.01^{+0.18}_{-0.23}$
3.60	2962.7(4)	2961.5(4)	−0.05(9)	−0.01(7)	0.04(7)	3558→596	$0^+ \to 1^+ \to 2_1^+$	$-2.2^{+0.5}_{-0.7}$
								$-0.14^{+0.10}_{-0.12}$
3.90	2673.6(6)	2670.7(7)	0.39(31)	0.28(20)	−0.12(32)	3875→1204	$0^+ \to 1^+ \to 2_2^+$	$\leqslant -4$
								$0.27^{+0.28}_{-0.26}$
								$\geqslant 5$
	3103.6(7)	not detected	−0.40(22)	0.57(36)	0.79(29)	Unknown		
4.03	2864.7(7)	2864.3(5)	−0.09(24)	0.01(19)	0.10(19)	4070→1204	$0^+ \to 1^+ \to 2_2^+$	$-0.18^{+0.25}_{-4.24}$
	2881.7(9)	2880.1(6)	0.07(25)	0.35(25)	0.29(28)	4084→1204	$0^+ \to 1^- \to 2_2^+$	$-0.47^{+0.35}_{-1.88}$
	3410.2(14)	3410.6(8)	0.11(29)	0.24(24)	0.14(29)	4006→596	$0^+ \to 1^- \to 2_1^+$	$-1.3^{+1.2}_{-1.5}$
	3478.36(15)	3478.2(7)	−0.17(45)	−0.16(31)	0.02(32)	Unknown		
4.18	3064.0(12)	3062.9(6)	0.08(31)	0.23(26)	0.15(29)	Unknown		
	3575.00(32)	3573.5(5)	−0.03(6)	−0.04(5)	−0.01(5)	4171→596	$0^+ \to 1^- \to 2_1^+$	$-2.9^{+0.4}_{-0.5}$
								$-0.04^{+0.04}_{-0.05}$
	3629.5(4)	3628.2(5)	−0.02(9)	−0.11(7)	−0.08(8)	4226→596	$0^+ \to 1^- \to 2_1^+$	$-3.6^{+0.8}_{-1.0}$
								$0.02^{+0.06}_{-0.062}$
4.34	3095.7(11)	3095.8(5)	0.21(29)	−0.12(16)	−0.33(19)	4301→1204	$0^+ \to 1^- \to 2_2^+$	$-4.8^{+2.4}_{-9.6}$
								$0.09^{+0.14}_{-0.18}$
							$0^+ \to 1^+ \to 2_2^+$	$\leqslant -2$
								$0.12^{+0.24}_{-0.29}$
								$\geqslant 18$
4.51	3898.1(7)	3896.7(6)	0.03(6)	−0.04(5)	−0.07(5)	4494→596	$0^+ \to 1^- \to 2_1^+$	$-2.8^{+0.4}_{-0.5}$
								$-0.05^{+0.04}_{-0.05}$
4.68	3560.4(18)	3558.5(11)	−0.27(58)	−0.40(37)	−0.15(29)	Unknown		
	4166.6(18)	4165.8(14)	0.09(37)	−0.24(24)	−0.33(29)	Unknown		
4.86	4230.0(4)	4229.2(6)	−0.04(7)	−0.09(6)	−0.05(6)	4826→596	$0^+ \to 1^- \to 2_1^+$	$-3.4^{+0.5}_{-0.7}$
								$0.00^{+0.05}_{-0.05}$
	4305.6(4)	4303.8(6)	−0.07(5)	−0.06(4)	0.01(5)	4900→596	$0^+ \to 1^- \to 2_1^+$	$-3.3^{+0.4}_{-0.4}$
								$-0.009^{+0.034}_{-0.034}$
	4343.7(5)	4342.5(7)	−0.00(8)	−0.32(6)	−0.32(7)	4939→596	$0^+ \to 1^- \to 2_1^+$	$-9.9^{+3.2}_{-7.7}$
								$0.19^{+0.05}_{-0.04}$
5.24	3688.1(5)	3688.7(11)	−0.82(30)	−0.61(44)	0.43(15)	5170→1483	$0^+ \to 1^- \to 0_2^+$	Pure *E1*
	4018.8(8)	4020.1(12)	−0.23(27)	−0.20(21)	0.03(18)	5225→1204	$0^+ \to 1^+ \to 2_2^+$	$-0.4^{+0.4}_{-2.5}$
							$0^+ \to 1^- \to 2_2^+$	$-4.8^{+2.3}_{-8.4}$
								$0.08^{+0.13}_{-0.17}$
	4674.1(5)	4673.7(13)	0.07(11)	−0.09(9)	−0.16(11)	5269→596	$0^+ \to 1^- \to 2_1^+$	$-3.0^{+0.7}_{-1.0}$
								$-0.03^{+0.08}_{-0.09}$
5.44	4838.5(7)	4837.5(10)	0.04(3)	−0.07(3)	−0.11(3)	5435→596	$0^+ \to 1^- \to 2_1^+$	$-3.00^{+0.23}_{-0.23}$
								$-0.031^{+0.022}_{-0.025}$
	4889.9(7)	4889.0(8)	0.14(7)	−0.04(6)	−0.18(8)	5484→596	$0^+ \to 1^- \to 2_1^+$	$-2.3^{+0.4}_{-0.4}$
								$-0.12^{+0.06}_{-0.07}$
	4897.2(8)	4895.0(12)	0.07(11)	0.25(14)	0.19(18)	5491→596	$0^+ \to 1^- \to 2_1^+$	$-1.7^{+0.6}_{-0.6}$
								$-0.26^{+0.13}_{-0.24}$
	4920.5(9)	[a]	–	–	–	5515→596	$0^+ \to 1^{(-)} \to 2_1^+$	

[a]Interference in all but the parallel detectors ($\theta = 90^\circ$, $\phi = 0^\circ, 180^\circ$).

TABLE IV. Decay information for all ^{74}Ge levels studied in this experiment, including branching ratios (BR) and spin and parity assignments. Comments are provided under the "Notes" column.

E_i (keV)	J^π	BR	E_f (keV)	J^π (final)	Notes
3033.5(4)	$1^{(-)}$		0.0	0_1^+	[a]ENSDF J^π: 1
3091.22(30)	$1^{(+)}$		0.0	0_1^+	ENSDF J^π: $1^{(+)}$. $J = 1$ and 2^+ resonances at 3089.4(9) and 3094.18(14) keV in ^{72}Ge.
			1204.205(7)	2_2^+	[a]
3558.0(4)	1^+	0.654(17)	0.0	0_1^+	ENSDF J^π: $1^{(-)}$
		0.346(17)	595.847(6)	2_1^+	[a]
3648.48(22)	1^-		0.0	0_1^+	ENSDF J^π: 1^+ at 3647.9(7) and 1^- at 3647(10) keV
3874.9(3)	1^+	0.921(13)	0.0	0_1^+	[b]ENSDF J^π: 1^+
		0.078(13)	1204.205(7)	2_2^+	[a,c]
3960.12(13)	1^+		0.0	0_1^+	[c]
4006.3(4)	1^-	0.79(4)	0.0	0_1^+	ENSDF J^π: 1
		0.21(4)	595.847(6)	2_1^+	[a,c]
4069.7(5)	1^+	0.45(4)	0.0	0_1^+	[c]
		0.55(4)	1204.205(7)	2_2^+	[a,c]
4084.49(31)	1^-	0.73(4)	0.0	0_1^+	ENSDF J^π: 1^+
		0.27(4)	1204.205(7)	2_2^+	[a,c]
4171.16(28)	1^-	0.49(2)	0.0	0_1^+	ENSDF J^π: 1
		0.51(2)	595.847(6)	2_1^+	[a,c]
4186.4(6)	1^+		0.0	0_1^+	[a,c]
4225.58(21)	1^-	0.750(16)	0.0	0_1^+	ENSDF J^π: 1^-
		0.250(16)	595.847(6)	2_1^+	[a,c]
4301.1(6)	$1^{(+)}$		0.0	0_1^+	ENSDF: Level at 4305.8(13) keV with $J = 1$.
			1204.205(7)	2_2^+	[a,c]BR= 0.63(5), 0.72(4) if 4301 keV is $J^\pi = 1^-, 1^+$, respectively.
4392.1(6)	$1^{(-)}$		0.0	0_1^+	[a,c]
4493.9(5)	1^-	0.460(21)	0.0	0_1^+	[c]
		0.540(21)	595.847(6)	2_1^+	[a,c]
4669.5(7)	1^+		0.0	0_1^+	[a,c]
4700.7(6)	1^-		0.0	0_1^+	[a,c]
4825.75(31)	1^-	0.568(23)	0.0	0_1^+	[a,c]
		0.432(23)	595.847(6)	2_1^+	[a,c]
4862.3(6)	1^+		0.0	0_1^+	[c]
4900.42(30)	1^-	0.452(19)	0.0	0_1^+	[c]
		0.548(19)	595.847(6)	2_1^+	[a,c]
4938.66(30)	1^-	0.658(23)	0.0	0_1^+	[c]
		0.342(23)	595.847(6)	2_1^+	[a,c]
4949.9(5)	1^-		0.0	0_1^+	[c]
5025.1(5)	1^-		0.0	0_1^+	[a,c]
5064.4(6)	1^+		0.0	0_1^+	[a,c]
5129.0(7)	1^-		0.0	0_1^+	[c]
5148.1(4)	1^-		0.0	0_1^+	[a,c]
5170.7(4)	1^-	0.620(35)	0.0	0_1^+	[a,c]
		0.380(35)	1482.81(4)	0_2^+	[a,c]
5224.5(5)	$1^{(-)}$		0.0	0_1^+	[a,c]
			1204.205(7)	2_2^+	[a,c]BR = 0.39(5), 0.59(6) if 5225 keV is $J^\pi = 1^-, 1^+$, respectively.

TABLE IV. (*Continued.*)

E_i (keV)	J^π	BR	E_f (keV)	J^π (final)	Notes
5268.84(29)	1^-	0.858(21)	0.0	0_1^+	[c]
		0.142(21)	595.847(6)	2_1^+	[a,c]
5283.2(9)	$1^{(+)}$		0.0	0_1^+	[a,c]
5420.5(8)	1^-		0.0	0_1^+	[c]
5434.8(5)	1^-	0.685(12)	0.0	0_1^+	[b]ENSDF J^π: 1^-
		0.315(12)	595.847(6)	2_1^+	[a,c]
5484.2(7)	1^-	0.638(27)	0.0	0_1^+	Known doublet with spin 1 and $T_{1/2} = 0.075(11)$ eV.
		0.362(27)	595.847(6)	2_1^+	[a,c]
5490.6(7)	1^-	0.851(30)	0.0	0_1^+	Known doublet with spin 1 and $T_{1/2} = 0.087(17)$ eV.
		0.149(30)	595.847(6)	2_1^+	[a,c]
5514.8(8)	$1^{(-)}$		0.0	0_1^+	[b]ENSDF J^π: 1
			595.847(6)	2_1^+	[a,c]
5563.0(5)	1^-		0.0	0_1^+	[c]

[a]Level or decay branch not previously reported in Ref. [29].
[b]Used in energy calibration. Level energies are adopted from Ref. [35].
[c]Level or decay branch not previously reported in Ref. [35]

a ^{72}Ge contaminant in the target. Neither measurement observed a branch from the 3034-keV level adopted in Ref. [35].

As mentioned in the introduction above, a major objective of the present work is to provide new tests of the ability of large-scale shell-model calculations with recently proposed effective interactions to reproduce as many of the structural properties of ^{74}Ge as possible. This approach was originally applied in the case of ^{76}Ge because of the importance of this nucleus for neutrinoless double-beta decay ($0\nu\beta\beta$). It is extended here to ^{74}Ge, following the work of Refs. [24,25] indicating that the $0\nu\beta\beta$ matrix elements in ^{76}Ge can be calculated from those in ^{74}Ge when taking two-nucleon transfer components into account. The most recent experimental information for ^{76}Ge to be compared with the results of shell-model calculations involves data sets from $(n, n'\gamma)$ [41] and Coulomb excitation [13], respectively. The configuration interaction calculations were carried out in the jj44 model space described in detail in the Appendix of Ref. [41], and consists of the $0f_{7/2}$, $1p_{3/2}$, $1p_{1/2}$, $0g_{9/2}$ single-particle states for both protons and neutrons. The JUN45 [16] and jj44b Hamiltonians were used. Both of these have been widely applied for the description of nuclei in the $A = 60$–100 region. In the case of the ^{76}Ge$(n, n'\gamma)$ data, the two interactions were found to be successful in providing a detailed description of the properties up to spin $\approx$6 and an excitation energy of $\approx$3 MeV. This result includes level energies, spins, and parities, as well as transition probabilities and branching ratios. The calculations were also found to reproduce salient structural features such as the γ band and location of the mixed-symmetry 2^+ state. Furthermore, the comprehensive set of transition and static $E2$ matrix elements extracted from the measured differential Coulomb cross sections was reproduced equally well [13], and the agreement between the calculations and experiment supports a near-maximum triaxial deformation of the ground state of ^{76}Ge. In addition, the degree of softness of the asymmetry in ^{76}Ge and the ^{76}Se daughter nucleus was investigated using rotational invariants generated from the shell-model wave functions computed with the jj44b and JUN45 interactions, and the comparisons indicate a stiff triaxial deformation in ^{76}Ge and a soft triaxial potential for ^{76}Se.

The present data are part of the same program of extensive comparisons between theory and experiment, focusing now on ^{74}Ge. New data from Coulomb excitation [14] and from the $(n, n'\gamma)$ reaction [26] are becoming available, and the present NRF results provide the opportunity for testing the shell-model calculations further by extending the comparisons for low-spin states toward higher excitation energies.

Focusing first on the $J^\pi = 1^-$ levels, Fig. 4 compares the excitation energy and number of states seen experimentally (a) with those calculated with the two shell-model interactions (b,c). The JUN45 and jj44b interaction predict 25 and 23 $J^\pi = 1^-$ levels in the 3–5.5 MeV range, respectively, matching closely the 21 experimental states given firm

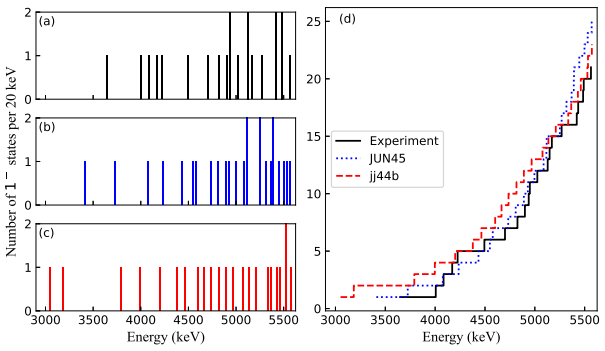

FIG. 4. Distribution of 1^- states (a) experimentally and calculated using (b) the JUN45 interaction and (c) the jj44b interaction. (d) shows a running sum of the number of states.

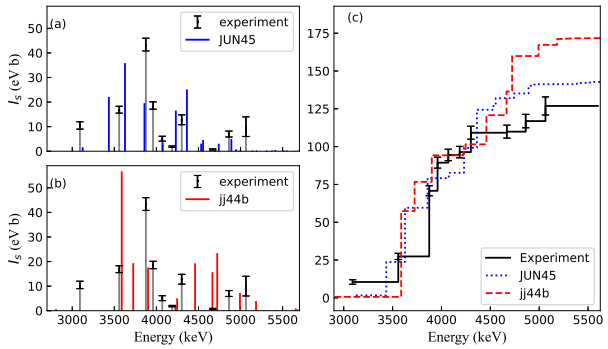

FIG. 5. Distribution of and cross-section values for experimental 1^+ states as compared to those calculated using (a) the JUN45 and (b) the jj44b interaction. (c) provides a running sum of the cross-section values.

$J^\pi = 1^-$ assignments in this work. More relevant at these high excitation energies is the distribution of the states as a function of excitation energy. Fig. 4(d) compares a running sum of experimental and calculated $J^\pi = 1^-$ levels as a function of excitation energy and illustrates the overall satisfactory agreement achieved with both effective interactions. All particle-hole states that give rise to the $E1$ strength distribution and, in particular, to the giant dipole resonance, lie outside the jj44 model space. This particle-hole strength mixes with the many-particle 1^- states within the jj44 model space to give rise to small $B(E1)$ values for these low-lying 1^- states. At present, there is no theoretical method to calculate this mixing. Therefore, observables such as values for the scattering cross section, branching ratios, and multipole mixing ratios for 1^- states have not been computed from theory, and only the distribution of states is presented in Fig. 4.

For the $J^\pi = 1^+$ states, the same reservations do not apply and experimental and theoretical cross-section data for excitation energies over the 3–5.5 MeV range are compared in Fig. 5. The effective $M1$ operator from Ref. [16] is used where the spin g factor is quenched by a factor of 0.7. The running sum of the cross section is given in Fig. 5(c). In the case of close-lying states, the sum of the associated $B(M1)$ probabilities and cross-section values is expected to reflect effects from mixing less than these quantities for the individual levels and is, therefore, more illustrative of the ability of the calculations to reproduce the data. As described previously, the cross-section data were obtained by linking the measured yields with those from Massarczyk *et al.* [29], which are smaller than the values from earlier measurements by Jung *et al.* [28] by 60–70 % on average. The resulting experimental sums in Fig. 5(c) are smaller than those predicted with the two shell-model interactions, but by 20–45 % only, justifying our comparisons based on the data of Ref. [29].

A close inspection of Fig. 5(c) indicates that the experimental running sum of scattering cross-section data to the $J^\pi = 1^+$ states appears to reach saturation, starting around 4 MeV in excitation energy, presumably reflecting the fact that the model space available for particle-hole excitations responsible for the positive-parity dipole states has been exhausted. The running sum calculated with the JUN45 interaction closely mirrors the data, while the jj44b sum predicts saturation at a slightly higher energy, closer to 4.5 MeV. The latter calculation also overestimates the value of the cross section at the highest energies.

It is worth noting that, at the lower excitation energies, some calculated shell-model states match the data closely, in terms of both cross sections and branching ratios. This is the case for the 3.558-MeV level observed with an elastic scattering cross section of 16.9(14) eVb, de-exciting toward both the 2_1^+ and the ground state with a branching ratio of 0.346(17) to the former. These properties are in close correspondence with those calculated with the JUN45 interaction for a 3.435-MeV state characterized by an elastic scattering cross section of 22.1 eVb and a branching ratio of 0.24 to the 2_1^+ yrast level. Associating results from the jj44b interaction with the data is somewhat more challenging for this particular state. In this instance, there are two predicted levels to consider: One at 3.588 MeV with a scattering cross section of 56.7 eVb and a branching ratio of 0.10 to the 2_2^+ level, and another at 3.725 MeV with corresponding values of 19.3 eVb and 0.36 to the 2_1^+ level. Based on the data of Table IV, it is possible that a 3.875-MeV state measured to have a 43.4(26) eVb cross section and a 0.078(13) branching ratio to the 2_2^+ level matches the data for the calculated 3.558-MeV level better. Similar comparisons between data and calculations can be made for many other levels, but one-to-one assignments become increasingly challenging as the density of states increases with excitation energy.

Generally speaking, the decay patterns for the $J = 1$ states observed in this work involve a dominating path toward the ground state with other branches feeding mostly the 2_1^+ state, the 2_2^+ level associated with the γ band, and the 0_2^+ level, i.e., the three lowest excited states with spin values readily reachable from the $J = 1$ levels excited in the NRF process. While this suggests a de-excitation process dominated by statistical decay, it is worth pointing out that at around 4.1 MeV in excitation energy, the data indicate a strong preference for de-excitation toward the 2_2^+ state with branching ratios on the order of 30–50 %. Calculations with both shell-model interactions also suggest favored decay paths toward the 2_2^+ level, but predict this to occur for states at somewhat higher energy: 4.2–4.5 MeV in the case of the JUN45 Hamiltonian and 4.5–5 MeV for jj44b.

From the discussion above it is clear that both effective interactions reproduce the dipole excitations in ^{74}Ge well. This result extends toward the higher excitation energy regime the conclusions reached for lower excitations on the basis of the recent $(n, n'\gamma)$ [26] and Coulomb excitation [13] studies. For all the data available from the three experiments, the two Hamiltonians reproduce the available data satisfactorily, although Ref. [13] indicates a slight preference for the jj44b interaction rather than the JUN45 one favored here. Coulomb excitation and neutron scattering data in ^{76}Ge led to similar conclusions.

V. CONCLUSIONS

Thirty-six $J = 1$ states in the ^{74}Ge nucleus, covering excitation energies between 3.1 and 5.6 MeV, were studied in this

work, exploiting the linearly polarized photon beams available at the HIγS facility and the NRF technique. Of these, 11 had not been reported previously [29], and 22 are also new with respect to the latest ENSDF compilation [35]. Firm J^π quantum numbers are assigned for 29 levels with tentative parities proposed for the others (see Table IV), resolving 16 ambiguities in parity with respect to earlier work. For ten of the states, results for the elastic cross section were inferred using the independent bremsstrahlung data from Massarczyk *et al.* [29].

The results provided an opportunity to test shell-model predictions in a domain relatively high in excitation energy. The jj44b and JUN45 effective interactions developed for nuclei in this mass region were found to be in good agreement with the experimental data, herewith extending toward higher excitation energies the conclusions reached in complementary $(n, n'\gamma)$ and Coulomb excitation studies. The JUN45 interaction was able to predict the total scattering cross section as well as some decay properties of the lowest-lying $J^\pi = 1^+$ states better than the jj44b Hamiltonian.

ACKNOWLEDGMENTS

We thank A. D. Ayangeakaa, C. Iliadis, and D. R. Gribble for their comments on this paper. This work is supported by the U.S. Department of Energy, Office of Science, Office of Nuclear Physics, under Grants No. DE-FG02-97ER41041 (UNC), DE-FG02-97ER41033 (Duke) and under Contract No. DE-AC52-07NA27344 (LLNL), and by the U.S. National Science Foundation under Grants No. PHY-2209178 (UK), PHY-1848177 (CAREER) (MSState), and PHY-2110365 (FRIB, MSU).

[1] K. Heyde and J. L. Wood, Rev. Mod. Phys. **83**, 1467 (2011).
[2] P. E. Garrett, M. Zielińska, and E. Clément, Prog. Part. Nucl. Phys. **124**, 103931 (2022).
[3] A. M. van den Berg, R. V. F. Janssens, G. T. Emery, A. Saha, and R. H. Siemssen, Nucl. Phys. A **379**, 239 (1982).
[4] R. Lecomte, M. Irshad, S. Landsberger, P. Paradis, and S. Monaro, Phys. Rev. C **22**, 1530 (1980).
[5] K. Nomura, R. Rodríguez-Guzmán, and L. M. Robledo, Phys. Rev. C **95**, 064310 (2017).
[6] A. A. B. Mennana, R. Benjedi, R. Budaca, P. Buganu, Y. E. Bassem, A. Lahbas, and M. Oulne, Phys. Scr. **96**, 125306 (2021).
[7] B. P. Crider, C. J. Prokop, S. N. Liddick, M. Al-Shudifat, A. D. Ayangeakaa, M. P. Carpenter, J. J. Carroll, J. Chen, C. J. Chiara, H. M. David, A. C. Dombos, S. Go, R. Grzywacz, J. Harker, R. V. F. Janssens, N. Larson, T. Lauritsen, R. Lewis, S. J. Quinn, F. Recchia *et al.*, Phys. Lett. B **763**, 108 (2016).
[8] S. M. Lenzi, F. Nowacki, A. Poves, and K. Sieja, Phys. Rev. C **82**, 054301 (2010).
[9] F. Nowacki, A. Poves, E. Caurier, and B. Bounthong, Phys. Rev. Lett. **117**, 272501 (2016).
[10] A. D. Ayangeakaa, R. V. F. Janssens, C. Y. Wu, J. M. Allmond, J. L. Wood, S. Zhu, M. Albers, S. Almaraz-Calderon, B. Bucher, M. P. Carpenter, C. J. Chiara, D. Cline, H. L. Crawford, H. M. David, J. Harker, A. B. Hayes, C. R. Hoffman, B. P. Kay, K. Kolos, A. Korichi *et al.*, Phys. Lett. B **754**, 254 (2016).
[11] Y. Toh, C. J. Chiara, E. A. McCutchan, W. B. Walters, R. V. F. Janssens, M. P. Carpenter, S. Zhu, R. Broda, B. Fornal, B. P. Kay, F. G. Kondev, W. Królas, T. Lauritsen, C. J. Lister, T. Pawłat, D. Seweryniak, I. Stefanescu, N. J. Stone, J. Wrzesiński, K. Higashiyama *et al.*, Phys. Rev. C **87**, 041304(R) (2013).
[12] A. D. Ayangeakaa, R. V. F. Janssens, S. Zhu, D. Little, J. Henderson, C. Y. Wu, D. J. Hartley, M. Albers, K. Auranen, B. Bucher, M. P. Carpenter, P. Chowdhury, D. Cline, H. L. Crawford, P. Fallon, A. M. Forney, A. Gade, A. B. Hayes, F. G. Kondev, Krishichayan *et al.*, Phys. Rev. Lett. **123**, 102501 (2019).
[13] A. D. Ayangeakaa, R. V. F. Janssens, S. Zhu, J. M. Allmond, B. A. Brown, C. Y. Wu, M. Albers, K. Auranen, B. Bucher, M. P. Carpenter, P. Chowdhury, D. Cline, H. L. Crawford, P. Fallon, A. M. Forney, A. Gade, D. J. Hartley, A. B. Hayes, J. Henderson, F. G. Kondev *et al.*, Phys. Rev. C **107**, 044314 (2023).
[14] N. Sensharma and A. D. Ayangeakaa (2023), (private communication).
[15] M. Hasegawa, T. Mizusaki, K. Kaneko, and Y. Sun, Nucl. Phys. A **789**, 46 (2007).
[16] M. Honma, T. Otsuka, T. Mizusaki, and M. Hjorth-Jensen, Phys. Rev. C **80**, 064323 (2009).
[17] S. J. Q. Robinson, L. Zamick, and Y. Y. Sharon, Phys. Rev. C **83**, 027302 (2011).
[18] D. J. Dean, K. Langanke, H. Nam, and W. Nazarewicz, Phys. Rev. Lett. **105**, 212504 (2010).
[19] P. A. Dar, R. Devi, S. K. Khosa, and J. A. Sheikh, Phys. Rev. C **75**, 054315 (2007).
[20] G. H. Bhat, W. A. Dar, J. A. Sheikh, and Y. Sun, Phys. Rev. C **89**, 014328 (2014).
[21] L. Gaudefroy, A. Obertelli, S. Péru, N. Pillet, S. Hilaire, J. P. Delaroche, M. Girod, and J. Libert, Phys. Rev. C **80**, 064313 (2009).
[22] J. P. Elliott, J. A. Evans, V. S. Lac, and G. L. Long, Nucl. Phys. A **609**, 1 (1996).
[23] Z. H. Wang, J. Xiang, W. H. Long, and Z. P. Li, J. Phys. G **42**, 045108 (2015).
[24] B. A. Brown, M. Horoi, and R. A. Sen'kov, Phys. Rev. Lett. **113**, 262501 (2014).
[25] B. A. Brown, D. L. Fang, and M. Horoi, J. Phys.: Conf. Ser. **966**, 012017 (2018).
[26] E. E. Peters and S. W. Yates (2023), (private communication).
[27] R. Schwengner, R. Massarczyk, K. Schmidt, K. Zuber, R. Beyer, D. Bemmerer, S. Hammer, A. Hartmann, T. Hensel, H. F. Hoffmann, A. R. Junghans, T. Kögler, S. E. Müller, M. Pichotta, S. Turkat, J. A. B. Turko, S. Urlaß, and A. Wagner, Phys. Rev. C **105**, 024303 (2022).
[28] A. Jung, S. Lindenstruth, H. Schacht, B. Starck, R. Stock, C. Wesselborg, R. D. Heil, U. Kneissl, J. Margraf, H. H. Pitz, and F. Steiper, Nucl. Phys. A **584**, 103 (1995).
[29] R. Massarczyk, R. Schwengner, L. A. Bernstein, M. Anders, D. Bemmerer, R. Beyer, Z. Elekes, R. Hannaske, A. R. Junghans, T. Kögler, M. Röder, K. Schmidt, A. Wagner, and L. Wagner, Phys. Rev. C **92**, 044309 (2015).

[30] A. Zilges, D. L. Balabanski, J. Isaak, and N. Pietralla, Prog. Part. Nucl. Phys. **122**, 103903 (2022).
[31] H. R. Weller, M. W. Ahmed, H. Gao, W. Tornow, Y. K. Wu, M. Gai, and R. Miskimen, Prog. Part. Nucl. Phys. **62**, 257 (2009).
[32] B. Löher, V. Derya, T. Aumann, J. Beller, N. Cooper, M. Duchêne, J. Endres, E. Fiori, J. Isaak, J. Kelley, M. Knörzer, N. Pietralla, C. Romig, D. Savran, M. Scheck, H. Scheit, J. Silva, A. Tonchev, W. Tornow, H. Weller *et al.*, Nucl. Instrum. Methods Phys. Res. A **723**, 136 (2013).
[33] D. Gribble, C. Iliadis, R. V. F. Janssens, U. Friman-Gayer, Krishichayan, and S. Finch, Phys. Rev. C **106**, 014308 (2022).
[34] J. H. Kelley, J. E. Purcell, and C. G. Sheu, Nucl. Phys. A **968**, 71 (2017).
[35] B. Singh and A. R. Farhan, Nucl. Data Sheets **107**, 1923 (2006).
[36] D. C. Radford, Nucl. Instrum. Methods Phys. Res. A **361**, 297 (1995).
[37] C. Romig, Investigation of Nuclear Structure with Relative Self-Absorption Measurements, PhD thesis, Technische Universität, Darmstadt (2015).
[38] C. Iliadis and U. Friman-Gayer, Eur. Phys. J. A **57**, 190 (2021).
[39] U. Friman-Gayer, Probing Nuclear Structure Relevant for Neutrinoless Double-Beta Decay with Nuclear Resonance Fluorescence, PhD thesis, Technische Universität, Darmstadt (2020).
[40] D. Abriola and A. A. Sonzogni, Nucl. Data Sheets **111**, 1 (2010).
[41] S. Mukhopadhyay, B. P. Crider, B. A. Brown, S. F. Ashley, A. Chakraborty, A. Kumar, M. T. McEllistrem, E. E. Peters, F. M. Prados-Estévez, and S. W. Yates, Phys. Rev. C **95**, 014327 (2017).